Sensor Covering

SteamVR™ Tracking

Introduction

Covering the sensors is an important aspect of the opto-mechanical design and should be considered a necessary part of productizing a tracked object. A cover prevents induced noise and malfunction of the sensor caused by contact with fingers or other objects. A covering also offers protection to the sensor from physical events such as impact, dust ingression, moisture ingression, and electrostatic discharge. It lastly improves the industrial design by concealing the sensors and other electronics.

This document will explore the topic of sensor coverings by first looking into how an individual sensor receives a signal from a base station. An equation will be derived to calculate the apparent centroid of a sensor from different incidence angles. Experimental modeling will then be used to explore how different covering configurations affect the ability to consistently determine the sensor centroid. The results lead to a discussion on best practices for architecture, geometry and materials.

Theory

SteamVR™ Tracking requires a base station, a tracked object, and a computer to track objects in virtual reality. A series of optical sensors on the tracked object receive IR laser sweeps from the base station. The laser is visible to the sensor for an amount of time dependent on the distance apart, relative orientation, laser sweep speed, and sensor position on the tracked object. Timestamps of when a laser strike begins and the strike duration are generated for each sensor. The times are sent to the computer and used to calculate estimates of the sensor centroids. The computer fits the estimated centroid locations to the actual locations on the tracked object. The translation and rotation values needed to establish this fit are then determined. A more comprehensive explanation of how SteamVR Tracking works can be found in the **System Overview** document.

The optical interaction between a base station and sensor can be analyzed with ray tracing and simple trigonometry. Light can be approximated as a ray, that is, an imaginary line directed along the path of the light. Rays can be extended from a base station to either end of a sensor to represent when the laser first and last hits a sensor. A diagram is shown below in Figure 1.

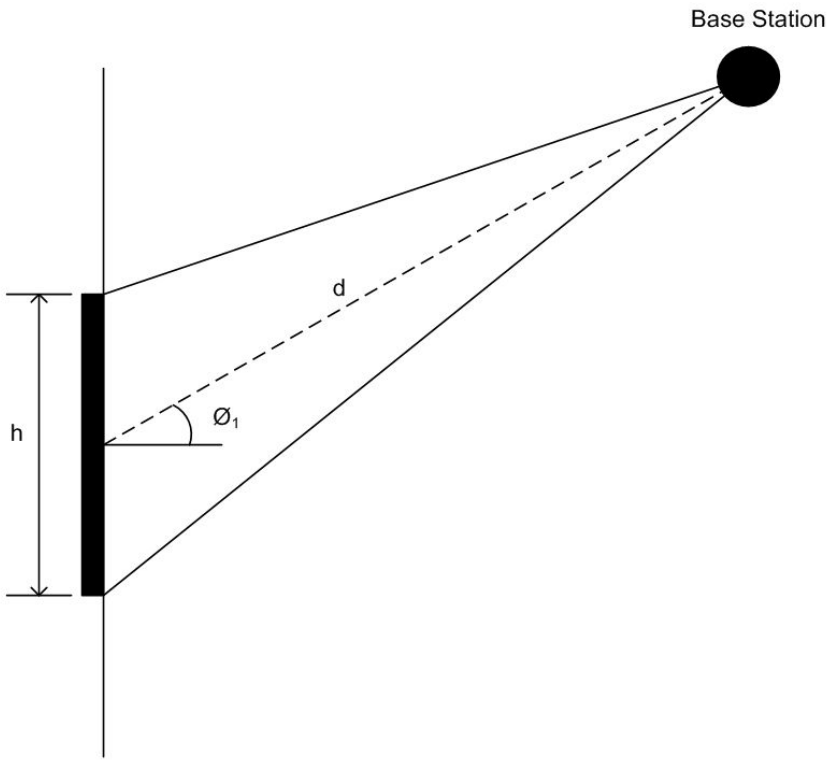

Figure 1

The height of the sensor is represented by h. If the sensor has no covering, h is the height of the photosensitive area. If the sensor has a covering, h is the the diameter of the outer surface of the cover. The distance and angle between the base station and sensor are d and $Ø_1$, respectively. In SteamVR Tracking, neither value is known until the estimated sensor centroids are fit to the actual sensor locations. This is all the information needed to calculate the angles over which a sensor is visible from the perspective of a base station.

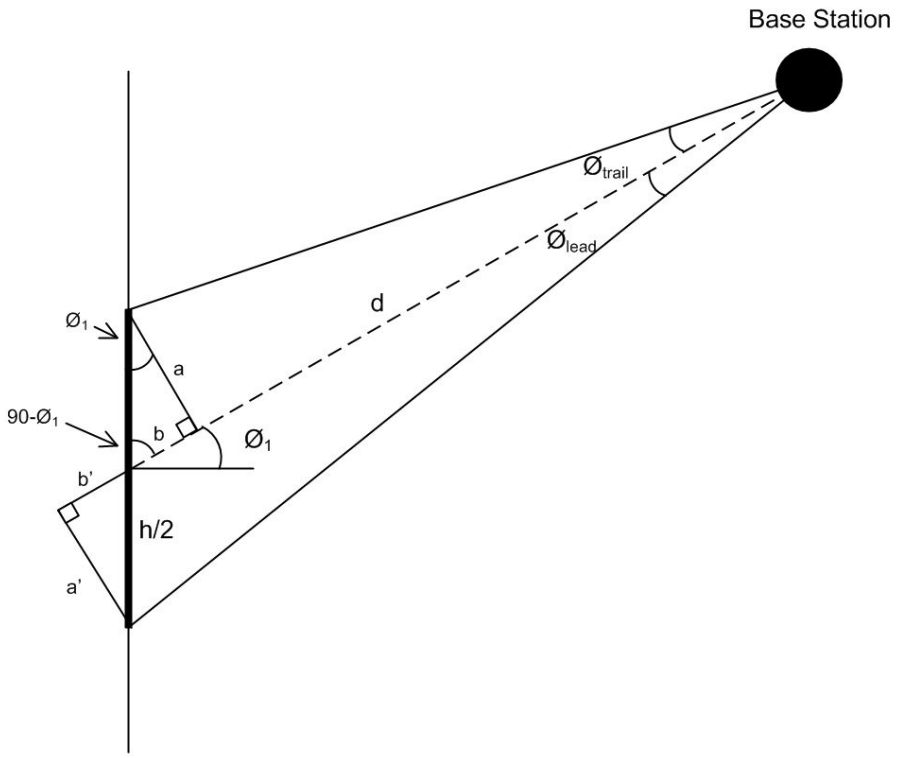

Figure 2

A centerline can be projected from the base station to the sensor centroid. Variables below the line are marked with the subscript “lead” while values above are marked with “trail.” These subscripts were chosen based on the direction of rotation of the base station y-sweep laser.

The angle for the trailing edge, $Ø_{trail}$, will be found first. A line is drawn perpendicular from the centerline to the trailing edge of the sensor. The angle nearest the sensor center in the newly formed triangle is complementary to $Ø_1$ and therefore:

$$90° - Ø_1 \quad (1)$$

The opposite angle is then equal to $Ø_1$. The length of sides a and b of the newly formed triangle can be calculated as follows:

$$cos\ Ø_1 = \frac{a}{h/2} \quad \rightarrow \quad a = \frac{h * cos\ Ø_1}{2} \quad (2)$$

$$sin\ Ø_1 = \frac{b}{h/2} \quad \rightarrow \quad b = \frac{h * sin\ Ø_1}{2} \quad (3)$$

The trailing edge angle can then be calculated.

$$Ø_{trail} = tan^{-1}\ \frac{a}{d-b} = tan^{-1}\ \frac{\left(\frac{h * cos\ Ø_1}{2}\right)}{\left(d - \frac{h * sin\ Ø_1}{2}\right)} \quad (4)$$

A similar derivation takes place to calculate $Ø_{lead.}$ The resultant formula is below.

$$\emptyset_{lead} = tan^{-1}\frac{a'}{d+b'} = tan^{-1}\frac{\left(\frac{h*cos\,\emptyset_1}{2}\right)}{\left(d+\frac{h*sin\,\emptyset_1}{2}\right)} \quad (5)$$

Angles calculated from equations 4 and 5 are small and can be difficult to interpret. Dividing the angles by the base station rotor speed results in the time needed for the laser to sweep through the angle. Multiplying the time by the computer clock speed yields the number of clock "ticks" over that timespan. The SteamVR Tracking system clock speed is 48 MHz while the base station lasers rotate at 60 Hz.

$$t\,[ticks] = \frac{\theta * f_{counter}}{\omega_{motor}} \quad (6)$$

$$f_{counter} = \frac{48\times10^6\ ticks}{1\ s} \quad (7)$$

$$\omega_{motor} = \frac{2\pi\ rad}{1\ cycle} \times \frac{60\ cycles}{1\ s} = \frac{120\pi\ rad}{1\ s} \quad (8)$$

Substituting equations 4, 5, 7, and 8 into 6 yields two new equations with angles converted to "ticks." A negative sign is added to t_{trail} to ease visualization when plotted.

$$t_{trail} = tan^{-1}\frac{\left(-\frac{h*cos\,\emptyset_1}{2}\right)}{\left(d-\frac{h*sin\,\emptyset_1}{2}\right)} * \left(\frac{48\times10^6}{120\pi}\right) \quad (9)$$

$$t_{lead} = tan^{-1}\frac{\left(\frac{h*cos\,\emptyset_1}{2}\right)}{\left(d+\frac{h*sin\,\emptyset_1}{2}\right)} * \left(\frac{48\times10^6}{120\pi}\right) \quad (10)$$

Equations 9 and 10 are plotted from -90 to 90 degrees in Figure 3. The blue lines above the y-axis represent the leading edge of the laser while the green lines below the y-axis represent the trailing edge. Measurements were taken from one to five meters between the base station and sensor. These values correspond to the target working range of the SteamVR system.

Observing the shape of the curves, a few takeaways can be made. First, the maximum number of ticks for the graph occur at an angle of 0 degrees and a distance of 1 meter. The distance between the base station and sensor is inversely related to the number of ticks. This is because the angular velocity of the laser sweep speed is constant but the tangential velocity changes based on the distance from the base station. Higher distances have a higher tangential velocity resulting in the laser sweeping across the sensor faster and the sensor registering fewer ticks. Second, the sensor registers no ticks at +/- 90 degrees. As the angle between the sensor and base station approaches 90 degrees, the projected area of the sensor visible to the base station decreases. At 90 degrees, the projected area is zero and no signal reaches the sensor.

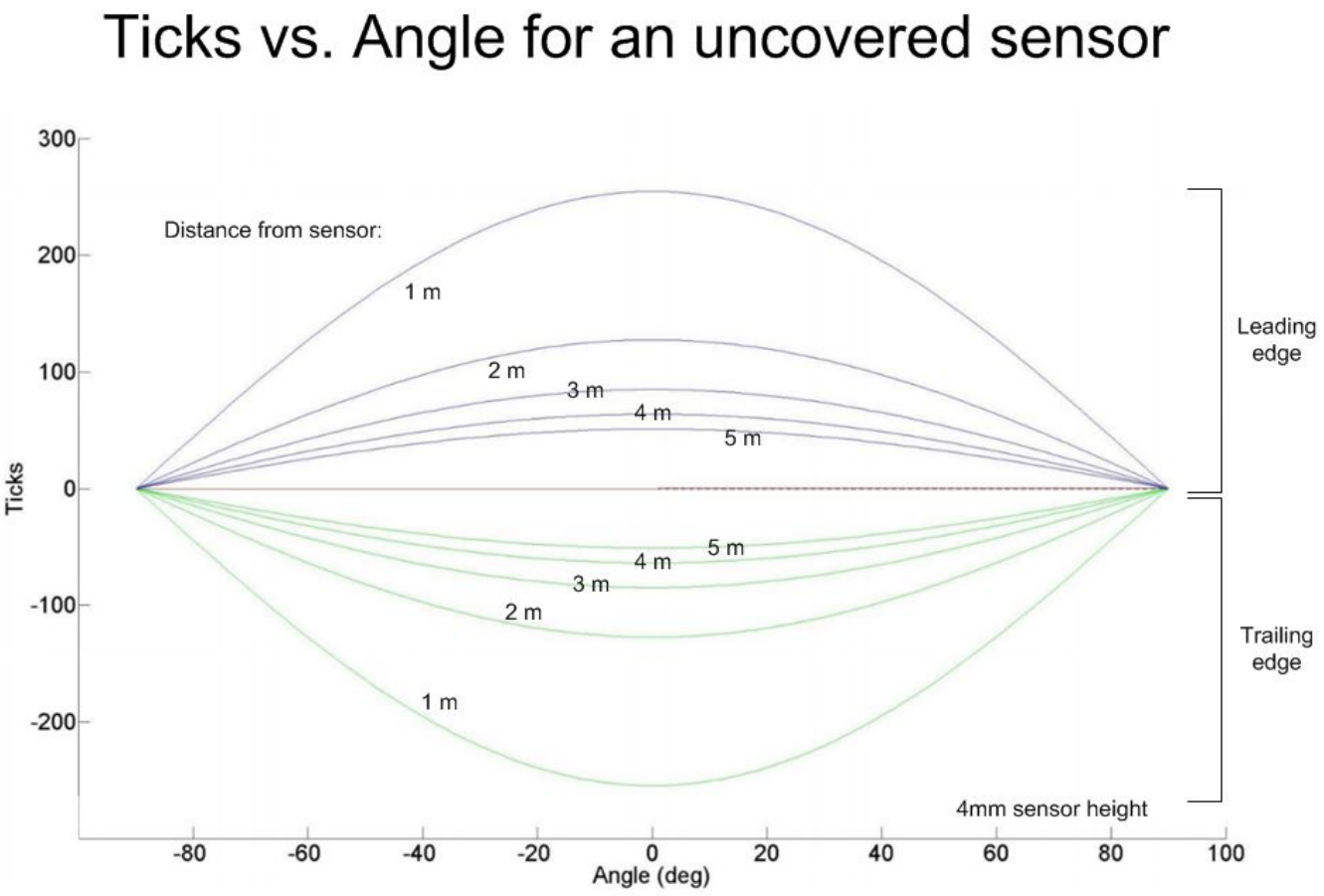

Figure 3

Experimental Results

Several experiments were conducted to characterize sensor performance with a variety of covering scenarios. The goal was to determine a set of sensor cover parameters that had minimal impact to system performance.

Setup

A test fixture was created to generate tick versus angle graphs for physical parts and covers. A base station was placed a constant distance from a sensor. The sensor was positioned facing and lined up with the output of the base station laser. The sensor angle was varied using a high accuracy rotation stage to generate number of ticks from -90 to +90 degrees. An illustration of the setup can be viewed in Figure 4. An image of the physical implementation of the fixture can be viewed in Figure 5.

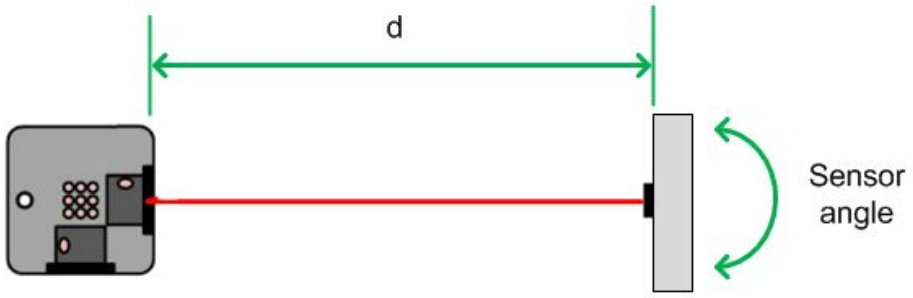

Figure 4

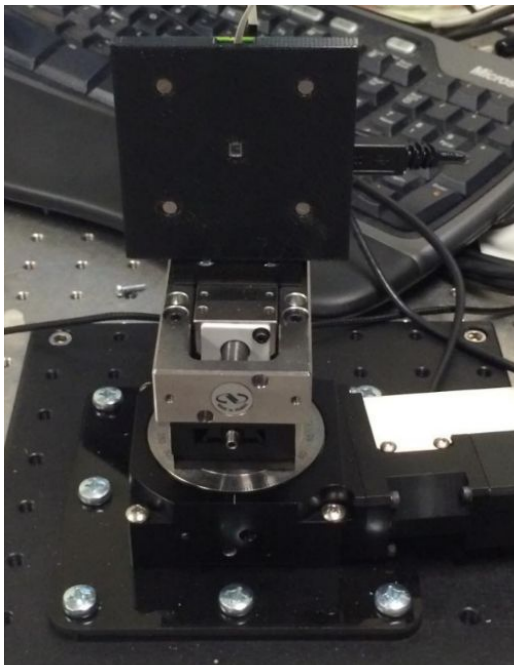

Figure 5

There is noise in the system due to variations in the laser rotor speed, electrical characteristics of the photodiode, and other minor effects. If the photodiode is not precisely aligned with the axis of rotation of the fixture, the effect of the alignment will be much greater than the effect to be measured. The fixture alignment can be calibrated by calculating the sensor centroid between -90 and +90 degrees. The setup assumes the sensor to be a point rotating about an axis. The calculated sensor centroid will have a specific curve shape depending on how far off center it is. The sensor position can be adjusted using an x-y stage on the fixture until the calculated centroid is flat over the entire range of angles recorded. Figure 6 shows what the curve for the calculated centroid looks like when the sensor location is offset in the direction along any axis of the graph. The curve for a properly calibrated test fixture is shown by the horizontal line in the middle-most graph.

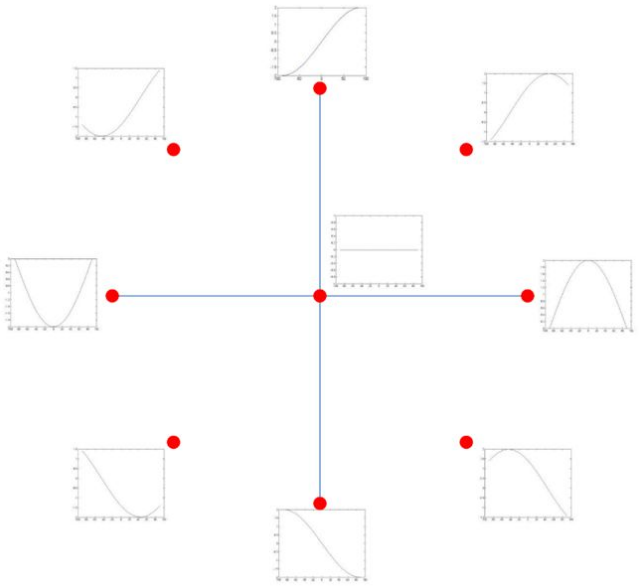

Figure 6

A series of covers were fabricated to be placed onto the fixture illustrated in Figure 5. The covers were used to test how different spacing, material thicknesses, and material optical properties affected the consistency of the measurement of the sensor centroid. Testing was conducted at approximately 650 nm with red lasers to make equipment sourcing and troubleshooting easier. Though the production base station emits its IR laser at a frequency of 830 nm, the experimental results will be the same as long as the optical properties are the same at the higher frequency. For example, use of a transparent material in the experiment means that it is transparent at 650 nm. To extend the results to the the production base station laser, the material must be transparent at 830 nm.

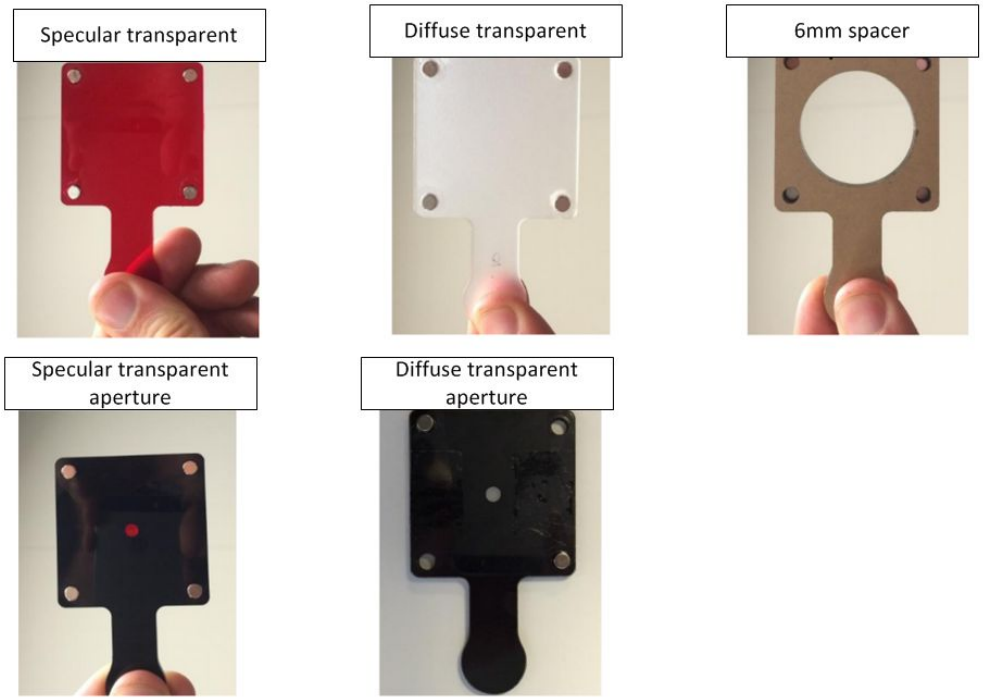

Figure 7

Three different types of materials were tested: specular transparent, diffuse transparent, and opaque. Transparency indicates that a majority of the target light wavelength passes through the material. An opaque material is one where light is not permitted to pass. A specular transparent material is one where light passes through it without being scattered. A diffuse transparent material is one where the light scatters in many different directions as it passes. See Figure 8 for illustrations of how light transmits through each of the materials used in the experiment.

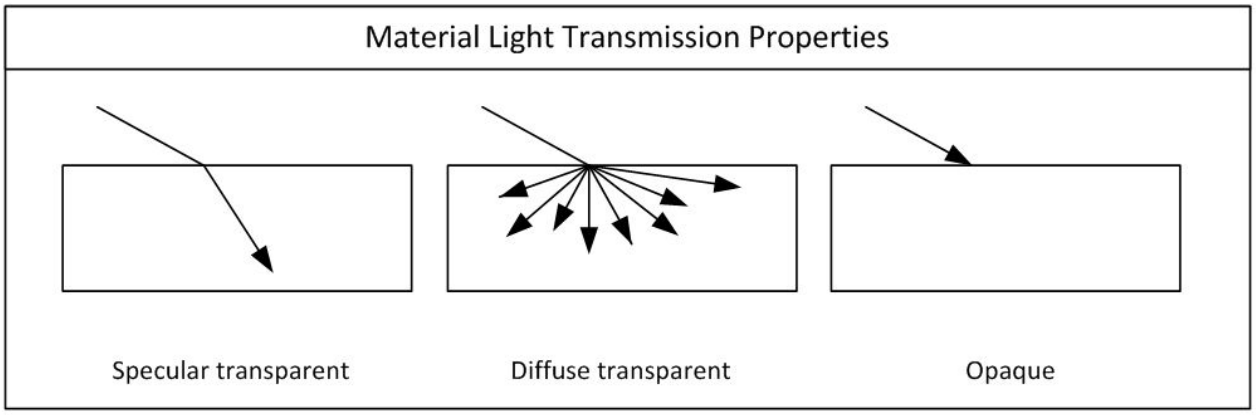

Figure 8

In addition to the materials, a spacer was used to position the photodiode either directly against the cover or 6mm away from it. An architecture with an aperture was also evaluated by placing a 4mm cylindrical plug of a transparent material in an opaque material. Images of each of the different test cases are shown in Figure 7.

Results

The covers were placed over the sensor in several different configurations. The base station and sensor were placed 2500mm apart and the experiment was run using the test fixture shown in Figures 4 and 5. Measurements were taken at 1 degree increments with 0.5 seconds spent at each increment. The centroid of the sensor was calculated for each setup and compared to the theoretical model. The results are contained in the plots in Figure 9. The blue dots represent the tick for the leading edge, the green dots represent the trailing edge, and the red dots represent the calculated centroid of the sensor. The gray curves underneath the dots represents the theoretical model.

Case #1: Uncovered

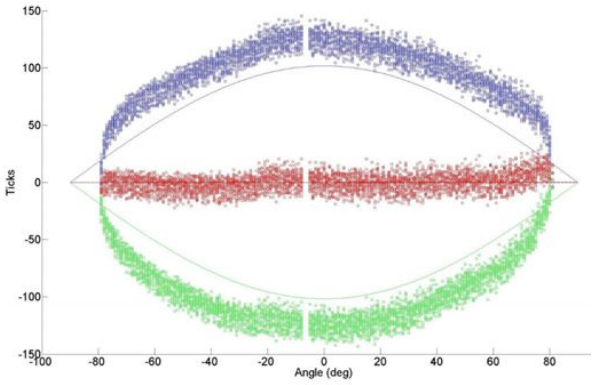

Cover material: None
Aperture diameter: Infinite
Cover thickness: 0 mm
Gap distance: 0 mm

Case #2: Specular transparent

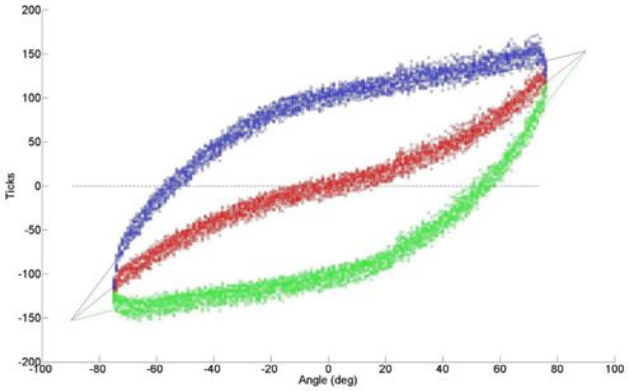

Cover material: Specular transparent
Aperture diameter: Infinite
Cover thickness: 3 mm
Gap distance: 0 mm

Case #3: Specular transparent

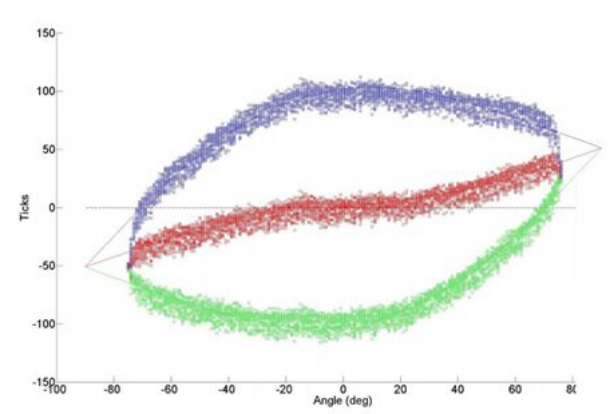

Cover material: Specular transparent
Aperture diameter: Infinite
Cover thickness: 1 mm
Gap distance: 0 mm

Case #4: Specular transparent + gap

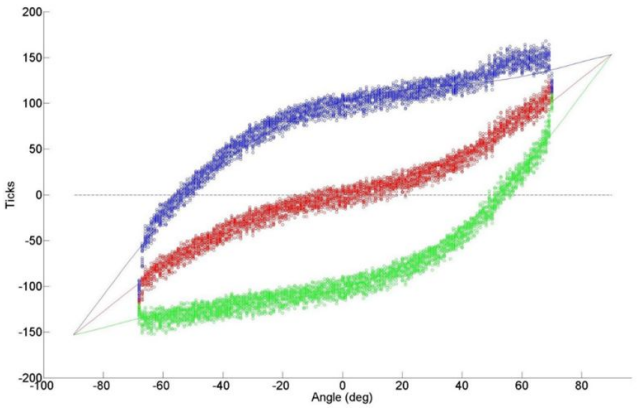

Cover material: Specular transparent
Aperture diameter: Infinite
Cover thickness: 3 mm
Gap distance: 6 mm

Case #5: Diffuse transparent

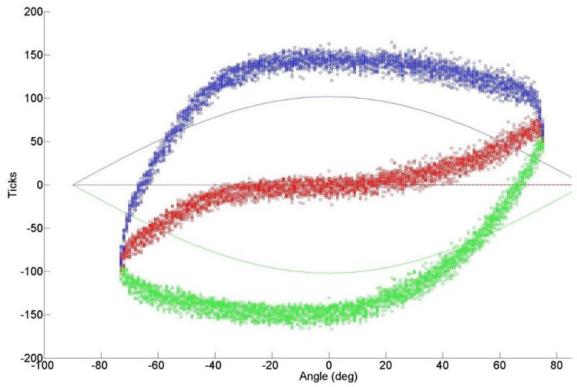

Cover material: Diffuse transparent
Aperture diameter: Infinite
Cover thickness: 1.5 mm
Gap distance: 0 mm

Case #6: Diffuse transparent + gap

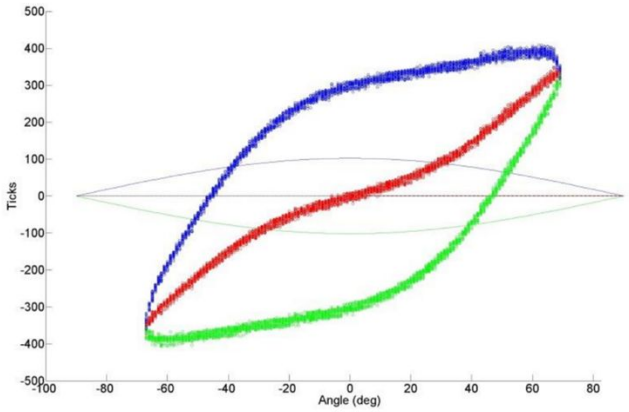

Cover material: Diffuse transparent
Aperture diameter: Infinite
Cover thickness: 1.5 mm
Gap distance: 6 mm

Case #7: Specular transparent aperture

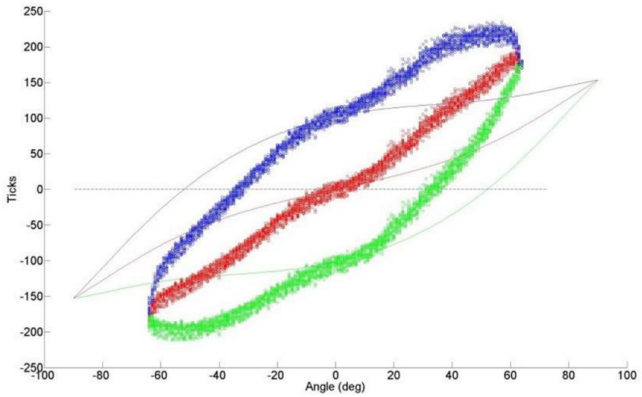

Cover material: Specular transparent
Aperture diameter: 4 mm
Cover thickness: 1.5 mm
Gap distance: 0 mm

Case #8: Diffuse transparent aperture

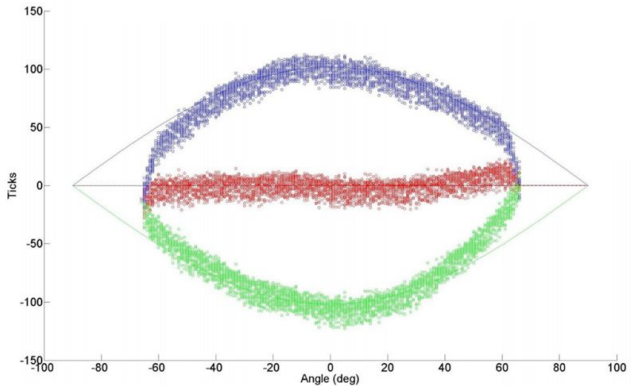

Cover material: Diffuse transparent
Aperture diameter: 4 mm
Cover thickness: 1.5 mm
Gap distance: 0 mm

Figure 9

Discussion

Case #1 considers a sensor with no cover over it. Leading and trailing ticks match the gray line representing the theoretical curve. The calculation of the sensor centroid is the most important value, however. Ideally the plotted sensor centroids at any angle should measure zero and form a flat line. Case #1 does this well but no values exist beyond +/- 80 degrees.

Truncation of results is apparent in most of the other cases as well for higher incidence angles. This is partially due to light reflecting away from the sensor. It is mostly due to not enough light getting to the sensor to activate it. At higher incidence angles, the projected area of the sensor visible to the base station is smaller. This is represented in a plot of the directional characteristics of the OSRAM BPW 34 S photodiode seen in Figure 10. Though the commonly assumed usable viewing angle of the photodiode is from -60 to 60 degrees it actually has sensitivity between -90 and 90 degrees. Expected sensitivity is 100% when the sensor is inline with the light source, 50% when 60 degrees off axis, and 20% when 80 degrees off axis. In the experimental setup of case #1 off axis at about 80 degrees, the sensitivity is too low to activate the sensor.

Directional Characteristics [1] *page 12*

$S_{rel} = f(\phi)$

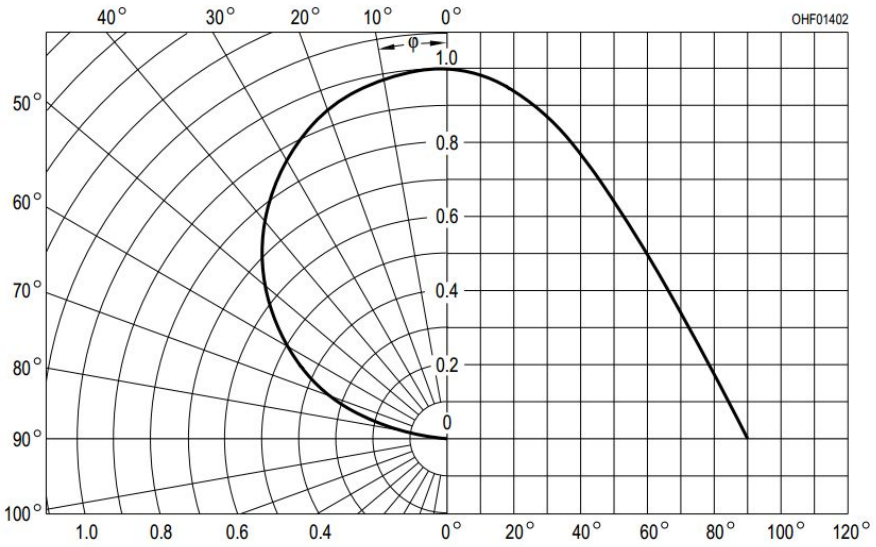

Figure 10

Another effect observed is that plotting the values of the leading and trailing number of ticks forms a wide line of data points. While some of this may be due to motor jitter, most is due to laser modulation. The laser is modulated at 1.8 MHz so that non-modulated light can be filtered out. Sensor samples are taken at the much faster clock speed of 48 MHz. The worst case, illustrated in Figure 11, is when the laser modulates off the moment before it sweeps over the sensor and a measurement is taken. The laser continues to sweep over the sensor surface until it modulates on 27 clock ticks later. At that point another sensor measurement is taken and the laser strike is recorded. The implication is that each sensor measurement can have up to 27 ticks of error associated with it. This appears on the graph as a wide line of data points. Though it may seem to be a substantial amount of error, enough measurements are taken that a good estimate of the actual value is able to be made.

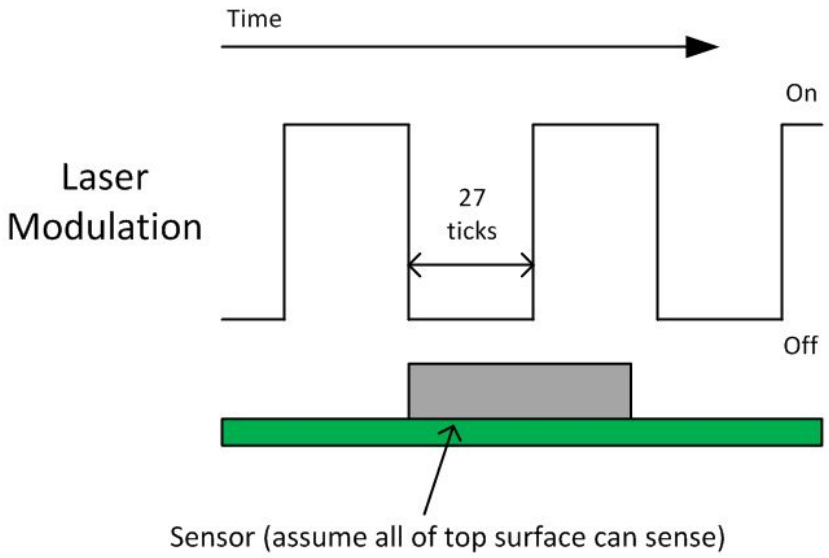

Figure 11

One last effect for case #1 is a notch of missing data occurring around -10 degrees. The explanation is that the sensor was walked in front of during the test and a portion of the measurements were missed.

Case #2 considers a specular transparent material positioned directly on top of the sensor. Leading and trailing ticks match the gray line representing the theoretical curve, but the results are tilted in comparison to case #1. As the incidence angle deviates from zero degrees, the calculated centroid moves farther away from the actual sensor centroid. The reason this happens is due to how light refracts as it passes from one medium to another. The relationship is described by the Snell-Descartes law which relates the incoming and outgoing incidence angles of the light to the refractive index of the respective medium.

$$sin\theta_1 * n_1 = sin\theta_2 * n_2 \quad (11)$$

θ_1 is the incoming incidence angle and n_1 is the index of refraction for the first medium. θ_2 is the outgoing incidence angle and n_2 is the index of refraction for the second material. In the case of the experiment, the laser travels through air until it hits the polycarbonate cover. It then refracts and travels through the cover material. The index of refraction of air is 1.00 and polycarbonate is 1.60. If an incidence angle of 60 degrees is assumed, the light will refract to 32.8 degrees. This is illustrated in Figure 12 below.

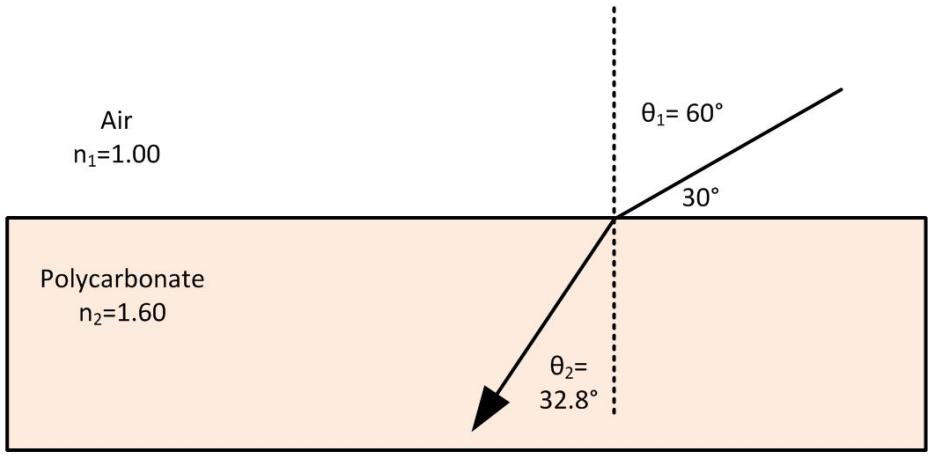

Figure 12

The amount that the laser light refracts in the cover material is thus closely tied to the incidence angle. At low angles, little refraction will occur while the refraction will be high for high angles. This concept is applied to the case #2 setup in Figure 13.

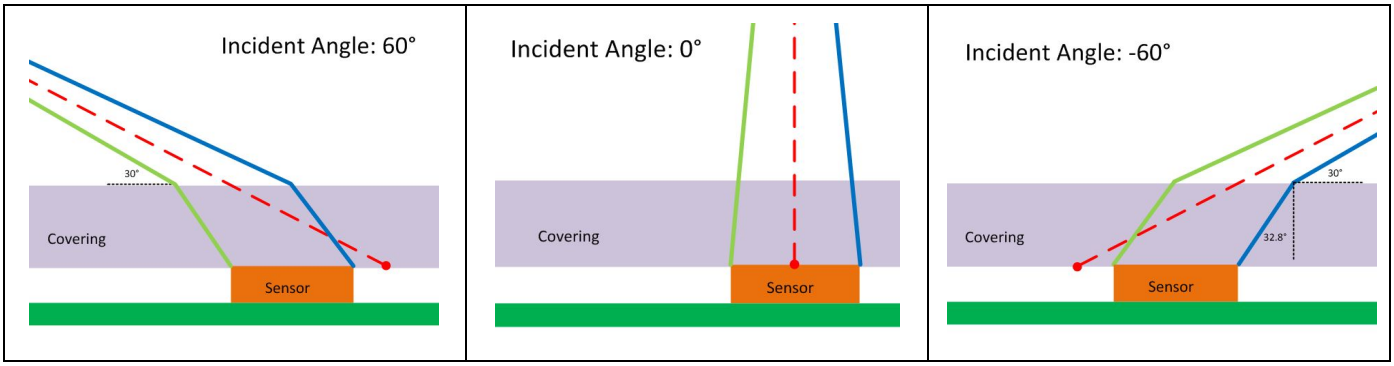

Figure 13

The blue line represents the ray trace of the laser that strikes the leading edge of the sensor while the green line corresponds to the trailing edge. The red dashed line represents a projected line from the light source to the calculated location of the sensor centroid. When the sensor surface is fully facing the laser, the calculated sensor centroid matches the actual sensor centroid. However, as the sensor incidence angle rotates to 60 or -60 degrees, refraction introduces error into the calculation. The calculated sensor centroid will effectively move across the face of the sensor as the orientation is changed, thus giving the shape observed in the case #2 result. Since the error is not constant over the range of incidence angles, it is difficult to calibrate out of the system.

Case #3 is similar to case #2 but the thickness of the cover material is reduced from 3mm to 1mm. At high incidence angles the light from the laser will still refract but since there is less material for it to travel through the effect will be less severe. The results are similar to case #2 but skewed less having smaller error at high incidence angles. If the cover material thickness is kept to a minimum, case #3 appears be a good covering strategy at low incidence angles.

Case #4 is similar to case #2 but the sensor is spaced 6mm from the cover material. As illustrated in Figure 14, the light from the laser refracts similarly when it leaves the air and transmits through the polycarbonate material. When the light leaves the cover material to traverse the air gap to the sensor it refracts again back to the original angle of incidence. When there is no aperture (i.e an infinite aperture) a ray trace shows that the resulting calculated sensor centroid is very similar to the illustration of case #2 in Figure 13.

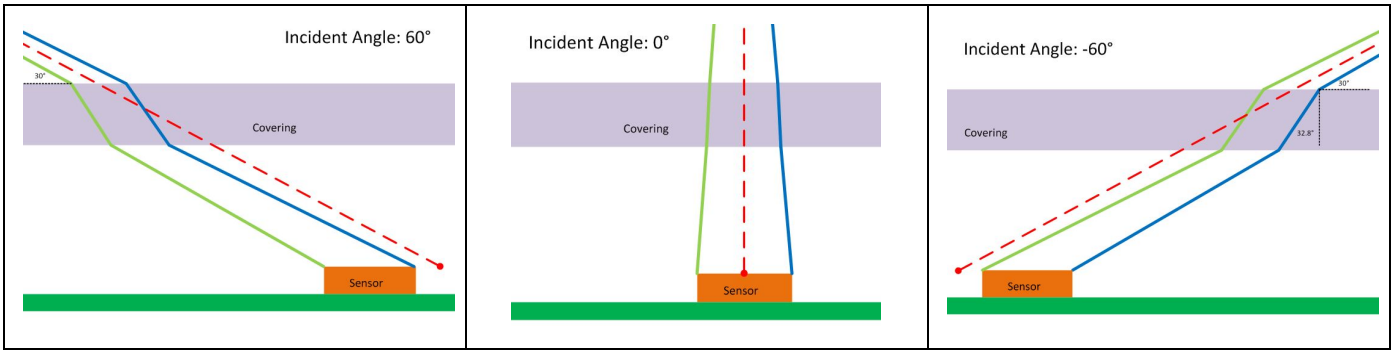

Figure 14

The calculated sensor centroid matches the actual sensor centroid when the sensor fully faces the laser. As the sensor rotation angle increases, refraction causes an error in the calculation of the sensor centroid. The plotted data for case #4 looks nearly identical to case #2.

Case #5 considers a diffuse transparent material positioned directly on top of the sensor. As shown in Figures 8 and 15, when the laser strikes a diffuse material, it will scatter in many different directions.

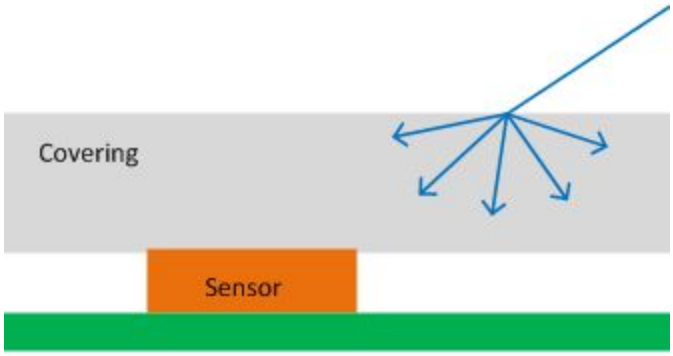

Figure 15

Since there is no defined aperture, the light can diffuse through the material far from the sensor. This leads to the sensor being activated prior to and after the laser is directly in line with the sensor. As a result there are errors in the calculation of the sensor centroid at higher incidence angles.

Case #6 is similar to case #5 but the sensor is spaced 6mm from the cover material. Also similar to case #5, the sensor is activated prior to and after the laser is directly in line with the sensor. The effect is further exaggerated by adding a space between the sensor and the cover. When the sensor was directly connected to the cover in case #5, only illumination of the portion directly above it could result in an activation. In case #6, the sensor is not connected to the cover and can be activated by illumination of adjacent portions of the cover.

One thing to note about any of the cases with a diffuse material is that at the time of this testing, the model describing light refraction for diffuse materials was not complete. This means that the gray theoretical curves for cases #5, #6, and #8 are incorrect and should be ignored.

Case #7 considers an opaque material with a 4mm diameter cylindrical plug of specular transparent material. The ray trace of the laser light is similar to case #2 except that the aperture is bounded by opaque material that doesn't allow light transmission. Just like in case #2, when the sensor faces the laser the calculated sensor centroid matches the actual sensor centroid. As the incidence angle increases, refraction causes error in the sensor centroid calculation. The opaque material surrounding the transparent plug blocks the light and removes some of the skewing of results that occurs at higher incidence angles.

Defining an aperture is a sizing exercise. When the aperture diameter is too large, it behaves the same as when there is no aperture, i.e. case #2. If the aperture is too small, the higher incidence angle results will be truncated. This may already be occurring for a 4mm diameter opening as there are only results from -65 to 65 degrees.

The physical geometry of the aperture may be causing error between the theoretical and actual results. The theoretical model assumes there is only refraction. The cylindrical plug geometry likely acts like a light pipe causing some light to reflect when it hits its the smooth walls.

Case #8 evaluates using an opaque material with a 4mm diameter cylindrical plug of diffuse transparent material. The laser light diffuses in the same way as discussed in case #5. The difference is that the diffuse material is constrained to be directly above the sensor. As shown in Figure 16, when the laser hits any of the outer portion of the diffuse material the light will travel through the entire volume triggering the sensor. There is a direct relationship between when the diffuse aperture receives a signal and when the sensor is activated. A diffuse material effectively moves the sensor location to the center of the outside surface of the aperture.

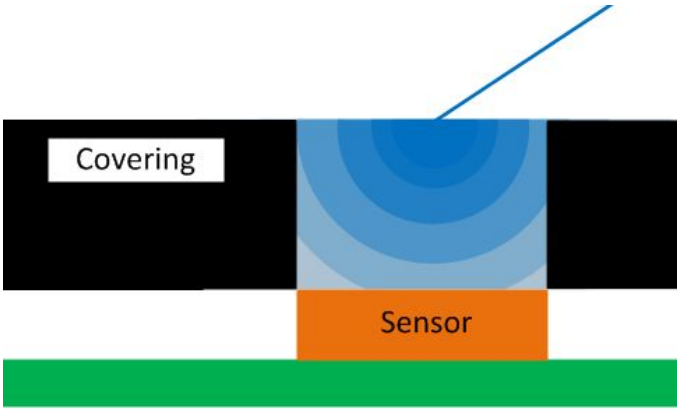

Figure 16

The case #8 plot looks better than any of the other covered architectures. The centroid of the sensor tracks the theoretical value accurately between -65 to 65 degrees. The diameter of the aperture may be too small as the results appear truncated at higher incidence angles. Increasing the diameter should resolve this but if it is made too large it will begin to act like there is no aperture, i.e. case #5.

Covering best practices

The results from the previously discussed experiments are condensed and summarized in the following sections.

Architecture

The most successful architecture is one where a sensor is positioned directly under an aperture formed from an IR transparent material. The aperture material should be surrounded by an IR opaque material. This architecture can be reduced to practice following the two main approaches illustrated in Figure 17.

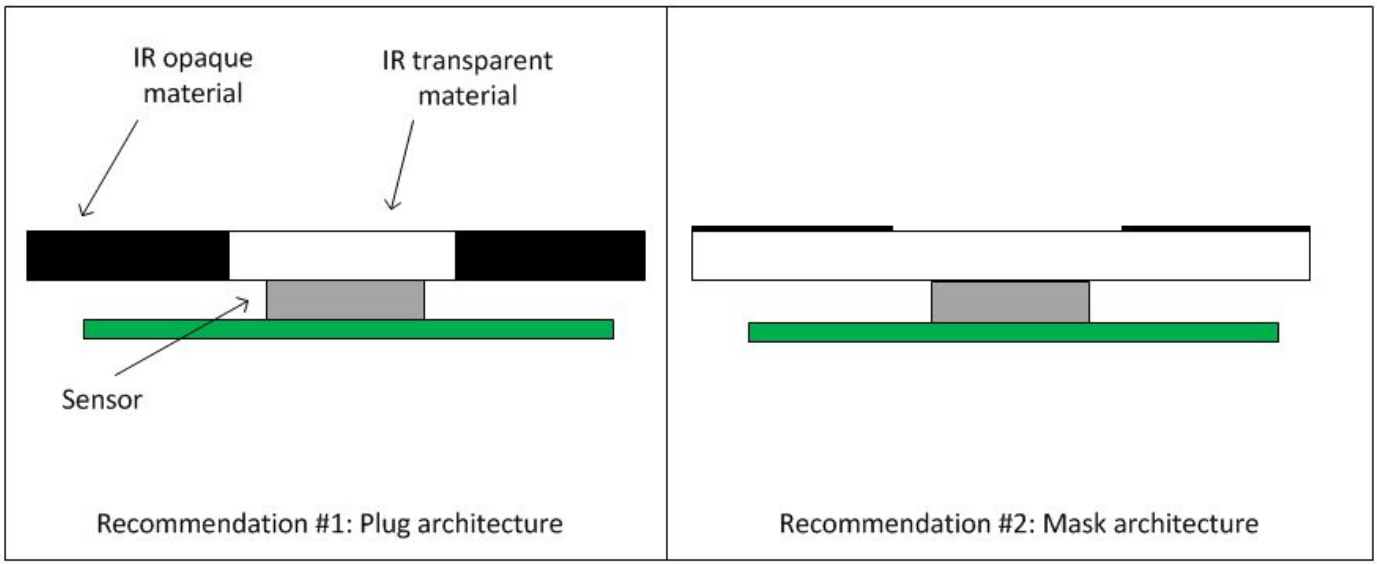

Figure 17

The plug architecture describes an IR opaque material holding an IR transparent plug of material to act as an aperture. The concept can be reduced to practice in a number of ways. The part could be injection molded using plastics with the desired optical properties in a two-shot process. The IR transparent material would be molded first with the IR opaque material molded onto it. Apertures can then be created by allowing the first material to show through in select areas. This was the approach taken in the design of the reference tracked object. A second approach is to create the housing out of an IR opaque material with physical holes in the sensor locations. IR transparent windows could be created out of a second part and attached to these holes. This approach is more expensive and time consuming to assemble but would have a lower injection molding tool cost and allows for the iteration of covering parameters.

The mask architecture is an alternative approach where an IR opaque mask is placed over an IR transparent material. This concept can be reduced to practice in several ways. One option is to injection mold the housing from a single, IR transparent material. The housing is then painted or coated by another means with an IR opaque substance. Apertures could be masked prior to coating or laser etched afterwards. Another option is to use an in mold label (IML) during injection molding to act as the mask layer. An IML restricts geometry of the final design but is lower cost than a two-shot injection molding approach.

There are a number of suboptimal architectures that are not recommended. The experimental results shown in Figure 9 indicate that it is hard for architectures with no apertures to accurately estimate the sensor centroid at high incidence angles. A variation on this is positioning a mask between the IR transparent material and the sensor. An opening in this type of mask would not prevent high incidence angle light from skewing the position of the calculated sensor centroid as shown in Figure 13.

Regardless what architecture is chosen, one should be selected as early in the design process as possible. Choosing one too late may increase the amount of time needed to complete the design. It may also change the manufacturing approach resulting in higher costs and longer lead times.

Aperture properties

Both of the recommended architectures require that the outer surface of the aperture be parallel with the top of the sensor. Curvature of the outer surface generally changes the field of view and causes the estimated sensor centroid to appear at different locations for high incidence angles. Having an aperture with high curvature like that on a sharp corner should be avoided. Slight curvature should yield acceptable results. Volumetric or surface diffusion on the aperture material may be required for this to work well. Any aperture geometry using curvature should be evaluated and tested before the design is finalized.

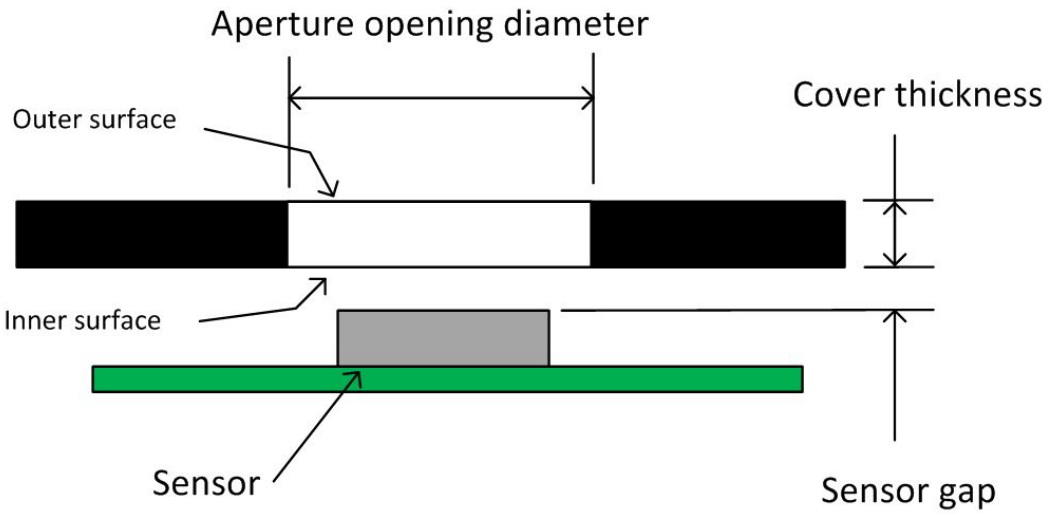

Figure 18

The aperture opening size is especially important. If it's too small not enough energy will be able to reach the sensor at high incidence angles. If it's too large, the system will act like there's no aperture at all and behave similar to the plots for cases #2 and #5 in Figure 9. A balance needs to struck to find the right size. A 6mm diameter opening is a good starting point. Larger windows can be used but the amount of aperture diffusion may need to be increased. The more diffusion added, however, the higher the level of attenuation. The result is that there might not be enough energy in a laser sweep to activate the sensor. One geometry not yet tested is that of a square opening. It theoretically should function but needs to be validated.

The thickness of the cover should be as thin as possible. Anything less than 1.0mm will work well. Getting the cover thinner is likely to be limited by the manufacturing method.

Diffusion of the cover material is desired and can be achieved in two different ways. The hardest way is by adding a diffusing element to the volume. Additives exist that can be added to the resin during the injection molding process. Unfortunately, most diffuse additives are designed to work with visible light and aren't effective at infrared frequencies. Additives that are effective at the desired frequency are laboratory grade, expensive, and only available in small quantities. A more economical way to add diffusion is by having a texture on the outer aperture surface. Most matte textures are likely to be effective and will likely be equivalent to volumetric diffusion. Regardless of what surface texture is selected, do not leave the finish glossy. SteamVR can robustly reject reflections off a mirror or window but reflections that occur close to the sensor obscure the real signal. A cover without any surface or volumetric diffusion can work but needs to be made as thin as possible to accurately estimate the sensor centroid. See the results case #2 and #3 in Figure 9 for further explanation. A cover with good diffusion can also be made thicker than recommended but increasing the thickness increases the signal attenuation. Not having enough signal energy could mean that the sensor won't activate when it should. The most robust architecture is to have a thin cover with a matte texture on the outside surface.

The surface finish on the aperture inner surface does not have a specific requirement. At the very least, machining marks should be removed to minimize noise as the light passes through. There is no recommendation for a specific surface finish on the aperture sidewalls. Glossy sidewalls will encourage the light to reflect and not be absorbed, much like in a light pipe. This increases the range that a tracked object will function from a base station but when close to a base station sensor saturation becomes more likely.

Sensor positioning

The gap between the sensor and inner surface of the aperture should be kept as small as possible. A large gap may cause high incidence angle light to miss the active area of the sensor.

The center of the sensor active area should be placed in the center of the aperture opening. Having it slightly offset no more than 0.5mm should work in most architectures but will cause decreased performance at high incidence angles. As shown by the mechanical outline in Figure 19, the center of the active area of the reference design sensor is offset 0.48mm from the center of the sensor package. An architecture with the sensor package centered to the aperture opening will therefore have the active area offset 0.48mm from the aperture.

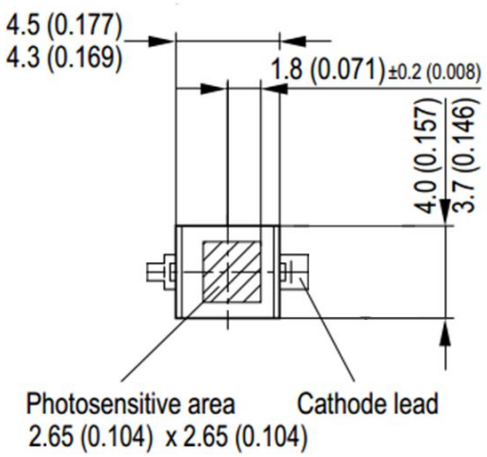

Figure 19

Sensor to sensor distance should be noted but hasn't been found to be too much of a problem. An initial concern with the reference design was that the signal from the laser would go into one aperture and trigger multiple sensors through a path of connected IR transparent material. Crosstalk such as this was never observed and is only expected to happen when there is very little distance between the sensors. Sensor placement 10mm apart is likely too far to have issues.

If the sensor must be moved away from the outer surface of the tracked object, care should be taken to ensure that the IR opaque material doesn't shadow the sensor at high incidence angles. As seen in Figure 10, the sensor has half the sensitivity at 60 degrees as it does at 0 degrees. 60 degrees is a good minimum viewing angle to target for occlusion avoidance. Projecting a line at 60 degrees from the edge of the sensor active area gives guidance on the minimum size and shape of the area needed to be kept free of obstructions. An illustration of the geometry constraints can be seen in Figure 20.

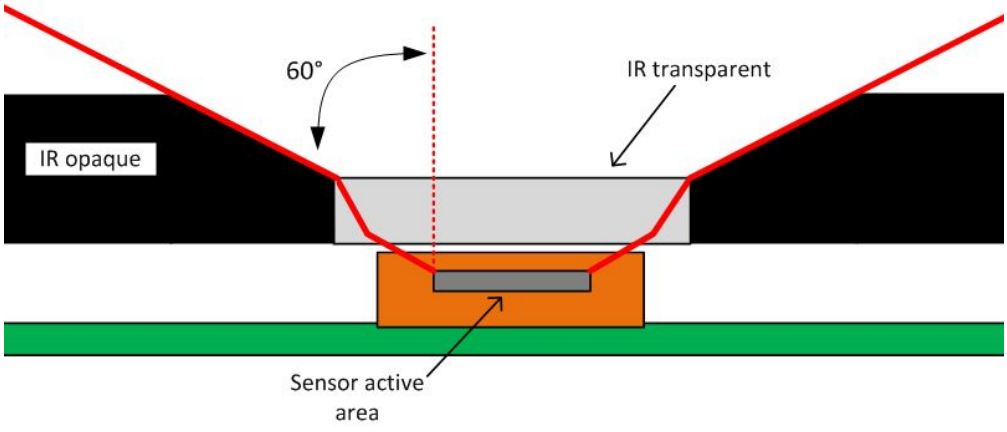

Figure 20

The evaluation should be done considering geometry at worst tolerances. Early in the design process this information might not be available and it may be safer to evaluate for occlusion at 70 degrees or greater.

A downside to this style of geometry is that new surfaces are created close to the sensor for light to reflect off of. If this light gets into the sensor, SteamVR will have a difficult time rejecting it. The finish on these new surfaces should be matte to minimize reflection.

Materials

The aperture material must be transparent to IR light. Polycarbonate (PC) and PMMA (acrylic) are good base material choices that generally meet this requirement. Indeed, most visibly transparent materials will be good for prototyping. Alone, however, they are inadequate for use in a final product.

The sensor can respond to light over a wide range of frequencies but SteamVR operates between 830 and 850nm. Testing has shown that high intensity flashes of visible light can saturate the sensor and affect tracking of an object in SteamVR. It thus makes sense to use the cover material as a filter only allowing the target frequencies through. Rejecting unused light frequencies makes the system more robust and takes some of the load off of the electrical and software systems. Ideally, the material would only let the target light frequencies pass but this would be an expensive solution. Several materials already exist that block visible light and allow anything higher (e.g. IR) to pass.

Materials with these performance characteristics can be created by including an additive in with the PC or PMMA during injection molding. The desired result of the additive is to block most of the visible light frequencies (400 - 700nm) while allowing most of the light at the target frequency to pass. Recommended transmission values at a normal incidence angle are 10% and 90% respectively. The numbers are not prescriptive, however, as materials with lower transmissivity values at the target frequencies have functioned acceptably. Most additives will turn the base material a dark color, usually black. Light grays and whites are not possible at this time.

There are fewer restrictions on the IR opaque materials. They should block most of the light at visible and target frequencies. Less than 1% transmissivity is recommended but not prescriptive as higher values could work. Most materials that are visibly opaque already do this. This generally allows them to be color matched to the IR transparent material. If the opaque material is going to be overmolded onto the IR transparent material, there needs to be approximately a 15 degree Celsius difference in the material melt temperature.

Fabrics haven't been explored much but should work if they are kept thin. Their results would likely match that of a diffuser with an infinite aperture (case #5 in Figure 9). If better results are desired, some sort of multi-material masking solution would have to be devised. Results would also be highly dependent on weave, thickness, and material specification. Extensive validation is needed for any sensor covering solution using fabrics.

A thin film or coating placed over the IR transparent aperture and surrounding opaque material could be a valid method to hide unwanted visible interfaces. The thickness of the film should be kept to a minimum, ideally less than 0.25mm. The outside of the film should have a matte texture to reduce reflection.

It's wise to generate transmission versus wavelength curves for each material used. How a material transmits visible light may be the same as it transmits IR but not always. Testing should be used for confirmation and can be a tool for potential debugging.

SABIC has shared the transmission curves for several of the IR opaque and transmitting LEXAN resins. The graphs are reproduced below in Figure 21 and in Appendix A with their permission. Please note their disclaimer that "each user bears full responsibility for making its own determination as to the suitability of SABIC Innovative Plastics materials, products, recommendations, or advice for its own particular use. Each user must identify and perform all tests and analyses necessary to assure that its finished parts incorporating SABIC-IP material or products will be safe and suitable for use under end-use conditions." The colors are available in several resin grades and each color is linked to its own set of grades. The ColorXPress search tool (https://www.sabic-ip.com/cxp/ColorXPress) can be used to find what grade a desired color is available in.

LEXAN Resin Transmission vs. Frequency
Color Code: 701
Color Description: Standard Opaque Black

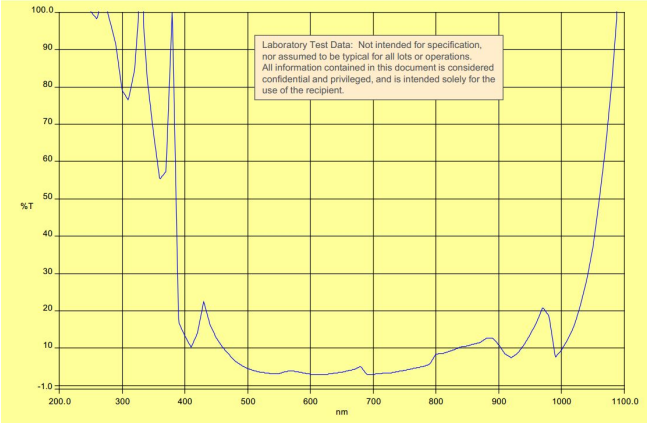

LEXAN Resin Transmission vs. Frequency
Color Code: BK1A184T
Color Description: IR Transmitting Black

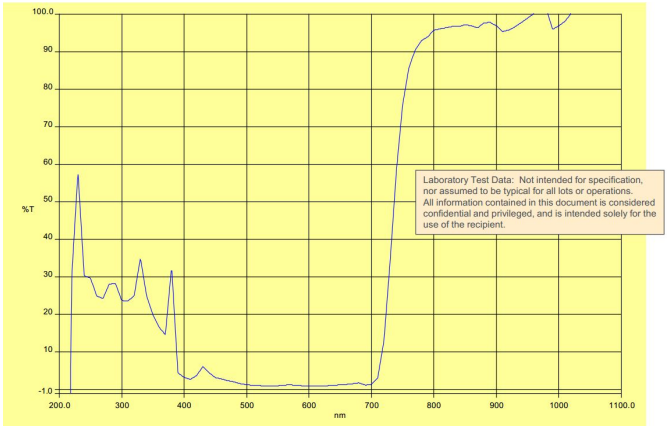

Figure 21

Figure 21 shows the transmissivity graphs for the IR opaque and transparent materials used the in the reference object. 701 was the color code used for the IR opaque material. Note that transmission is generally less than 10% over the visible spectrum (400 - 700nm) and target frequencies (830 - 850nm). BK1A184T was the color code used for the IR transparent material. Its transmission is generally less than 5% over the visible spectrum while being greater than 90% at the target frequencies.

Another material supplier to consider is Covestro. They have the graphs of several IR-transparent materials in the their “Optical properties of Makrolon and Apec for non-imaging optics” (http://www.plastics.covestro.com/Products/~/media/B6555362438341FF9804F21A253E5B23.ashx?la=en) document. Their representatives can offer guidance on material selection and provide samples. Whoever is selected, it’s a good practice to contact the material supplier to get the latest information and to further discuss the application. The correct grade of resin for a specific VR application is very dependent on the function and geometry of the part and should be tested to ensure suitability.

Reference Design Sensor Covering

A tracked object reference design was created for SteamVR. The sensors were covered according to the best practices outlined in the previous section. A summary of the covering properties is listed below. The definitions can be found in Figures 18 and 20. The values for the reference design are all nominal and don’t include tolerances.

	Tracked object reference design parameters
IR transparent cover thickness	1.0 mm
Aperture opening diameter	6.0 mm
Sensor gap	0.23 mm
Unobstructed viewing angle	62 degrees
IR transparent material	SABIC LEXAN FXE1414T - BK1A184T

IR opaque material	SABIC LEXAN HFD1711 - 701
Aperture outer surface texture	MT-11020
Minimum sensor centroid to sensor centroid distance	Approximately 15 mm

Figure 22

Conclusion

An opto-mechanical theory has been discussed to help understand the effects of different covering methods on tracking in SteamVR. An experimental setup was constructed and used to determine the actual effect given real world constraints. Several best practices were established from the theoretical and experimental models. Guidance was provided for architecture, aperture properties, sensor positioning, and materials. A good covering strategy is an important part of an object robustly tracking in SteamVR. Since it is so integral to the design it should be considered as early as possible.

Appendix A: Material Transmission vs. Frequency Data

LEXAN Resin Transmission vs. Frequency
Color Code: 111
Color Description: Standard Natural
Notes: High transmission visible and IR

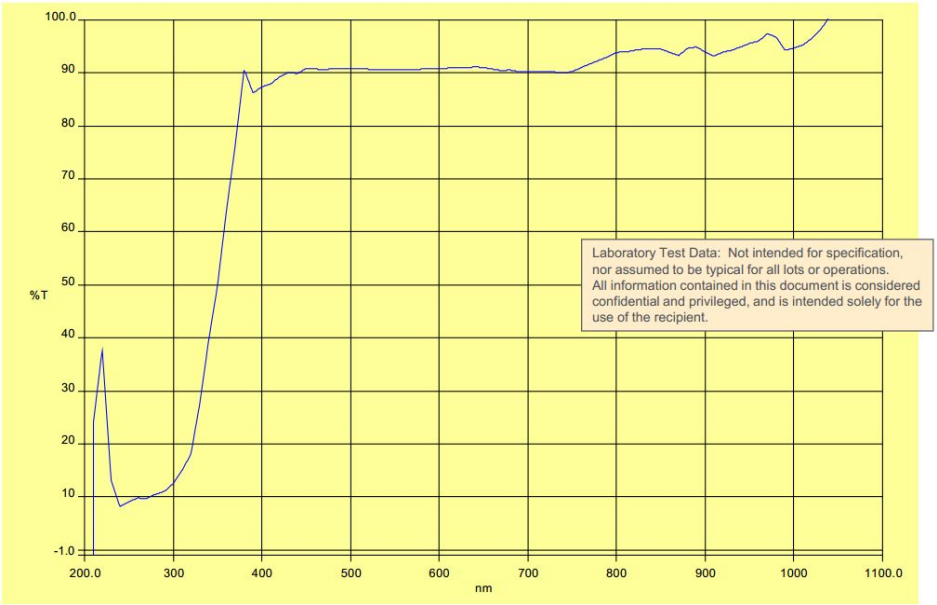

LEXAN Resin Transmission vs. Frequency
Color Code: 701
Color Description: Standard Opaque Black

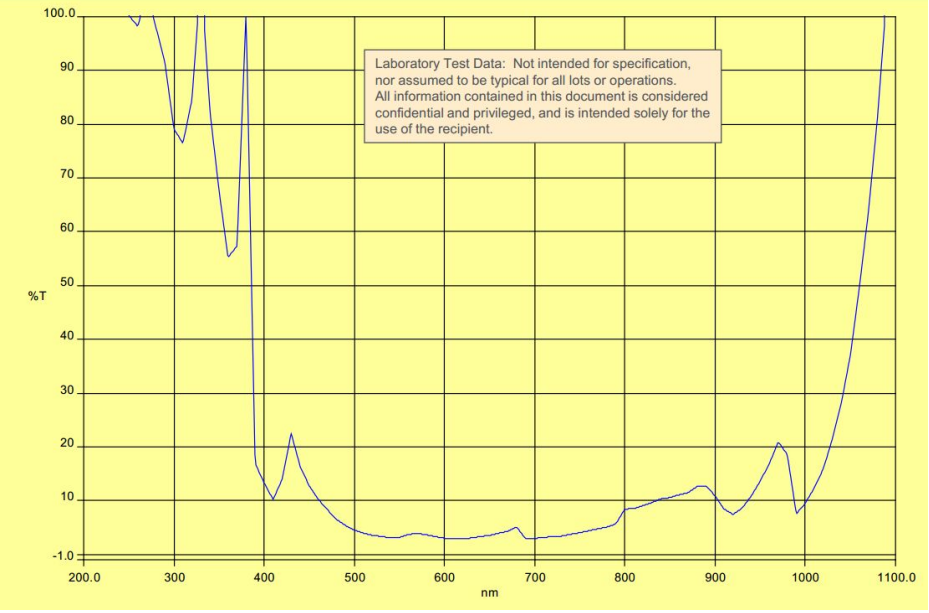

LEXAN Resin Transmission vs. Frequency
Color Code: 7H1D505T
Color Description: IR Transmitting Black
Notes: Healthcare

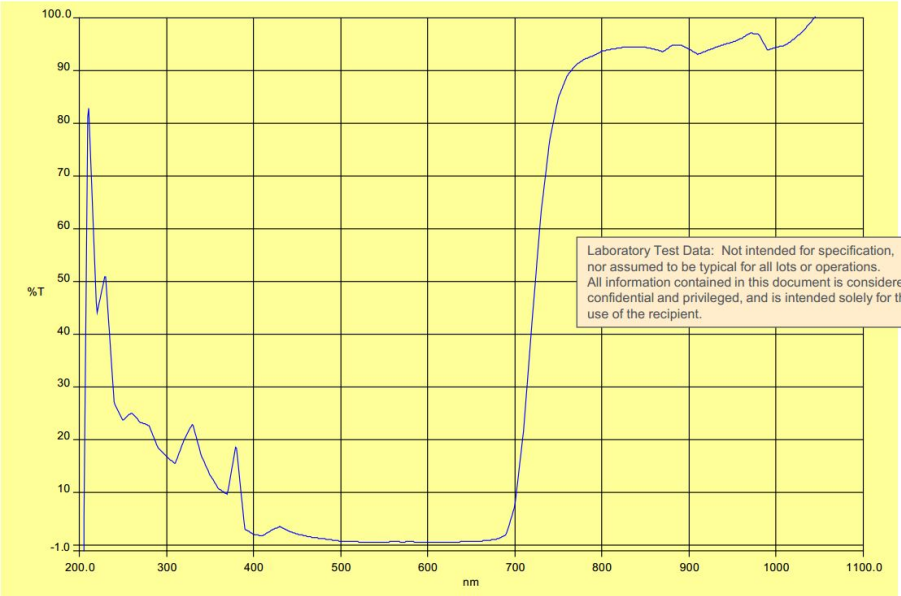

LEXAN Resin Transmission vs. Frequency
Color Code: 21051
Color Description: IR Transmitting Deep Blue

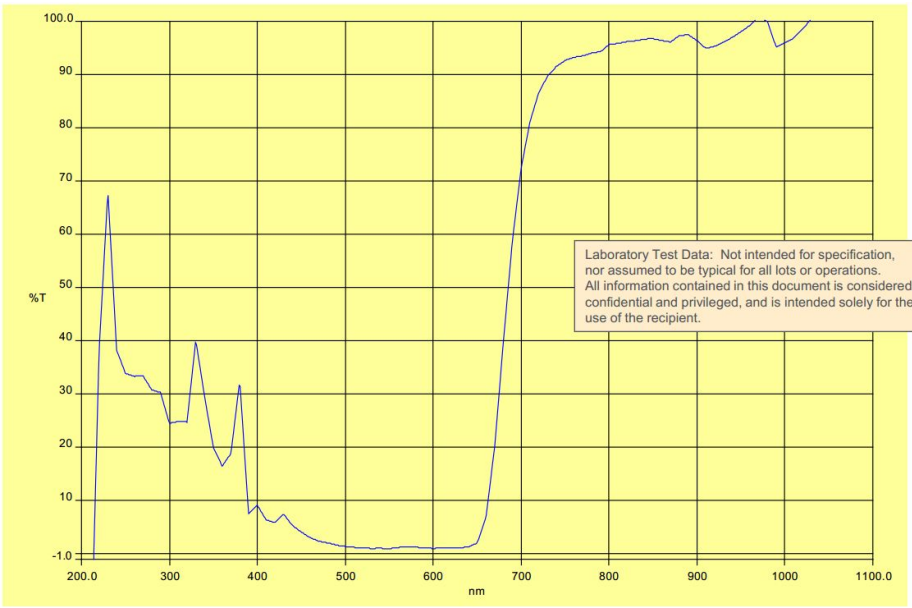

LEXAN Resin Transmission vs. Frequency
Color Code: 21064
Color Description: IR Transmitting Deep Blue

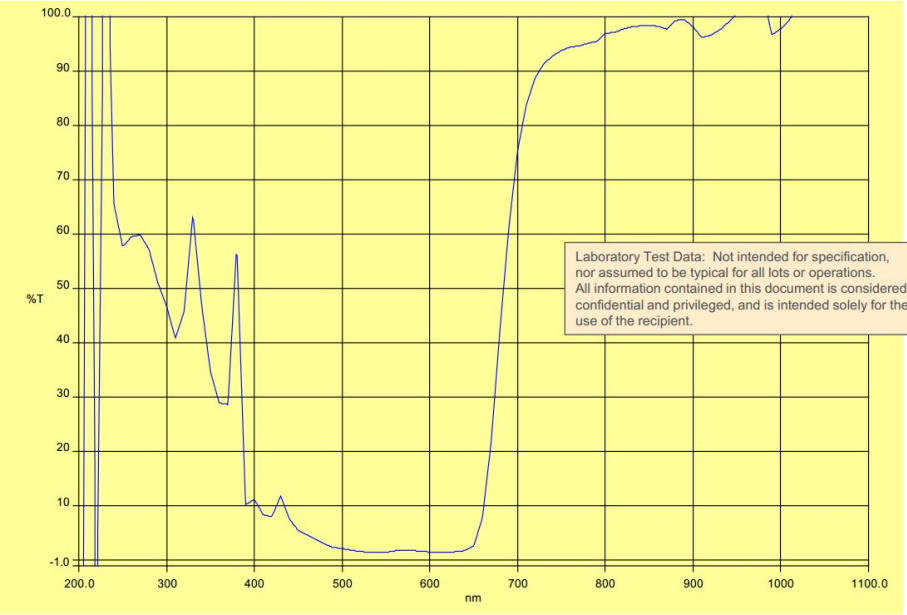

LEXAN Resin Transmission vs. Frequency
Color Code: 21092
Color Description: IR Transmitting Deep Blue

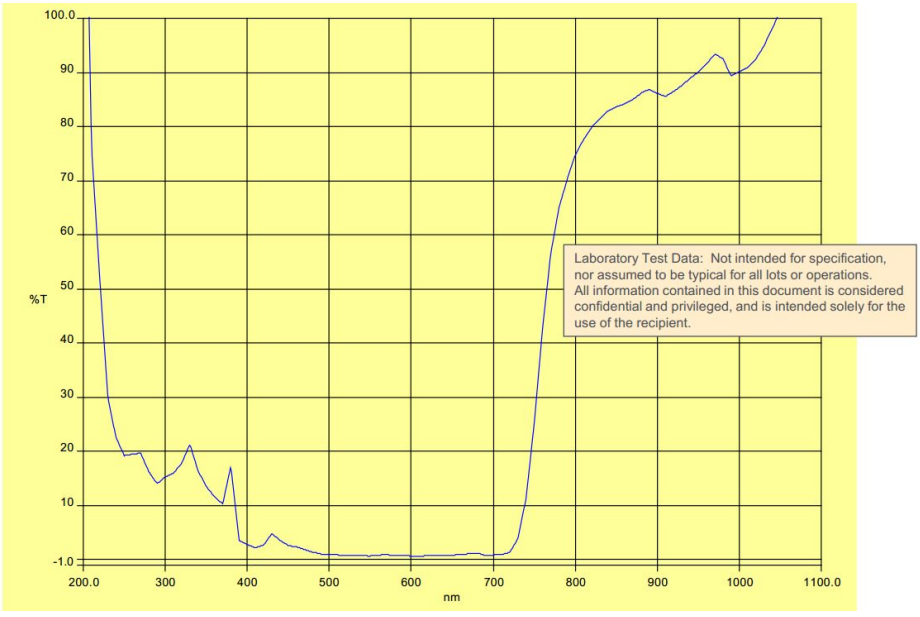

LEXAN Resin Transmission vs. Frequency
Color Code: 21125
Color Description: IR Transmitting Deep Blue

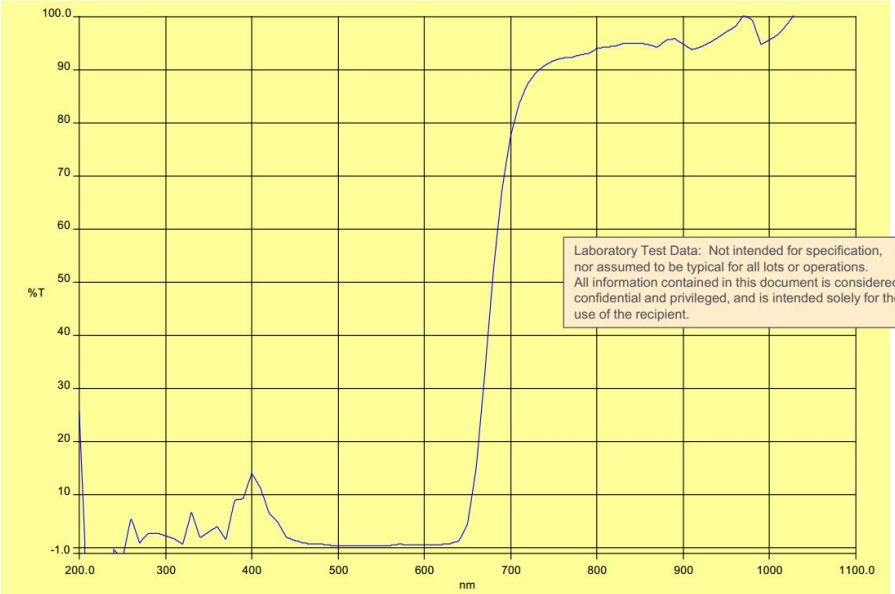

LEXAN Resin Transmission vs. Frequency
Color Code: 21127
Color Description: IR Transmitting Deep Blue

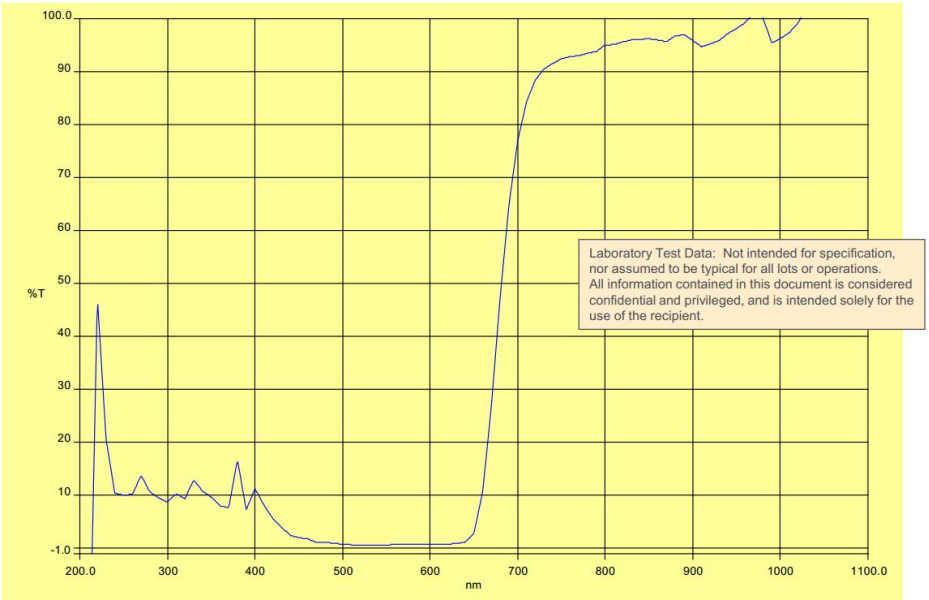

LEXAN Resin Transmission vs. Frequency
Color Code: 31142
Color Description: IR Transmitting Deep Green

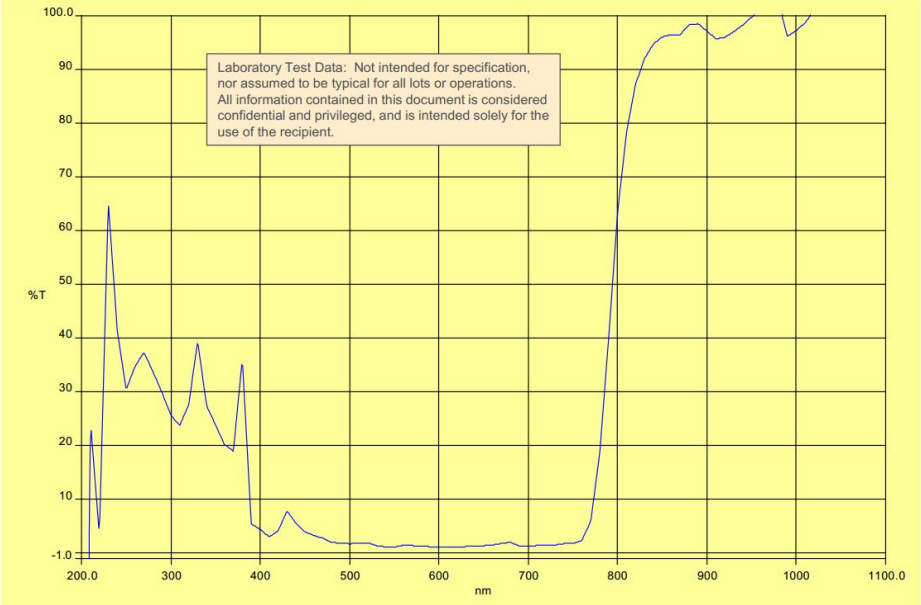

LEXAN Resin Transmission vs. Frequency
Color Code: 61028
Color Description: IR Transmitting Deep Red

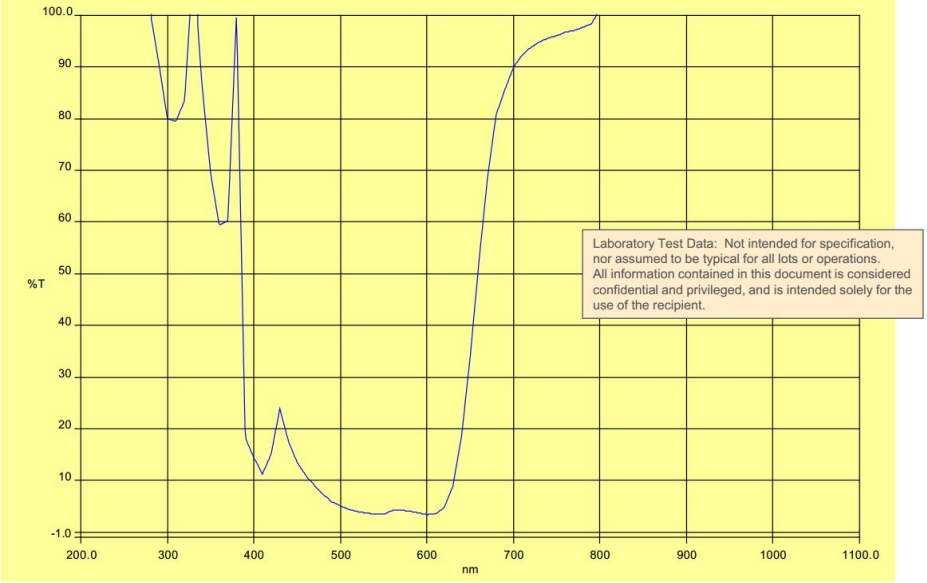

LEXAN Resin Transmission vs. Frequency
Color Code: 61036
Color Description: IR Transmitting Deep Red

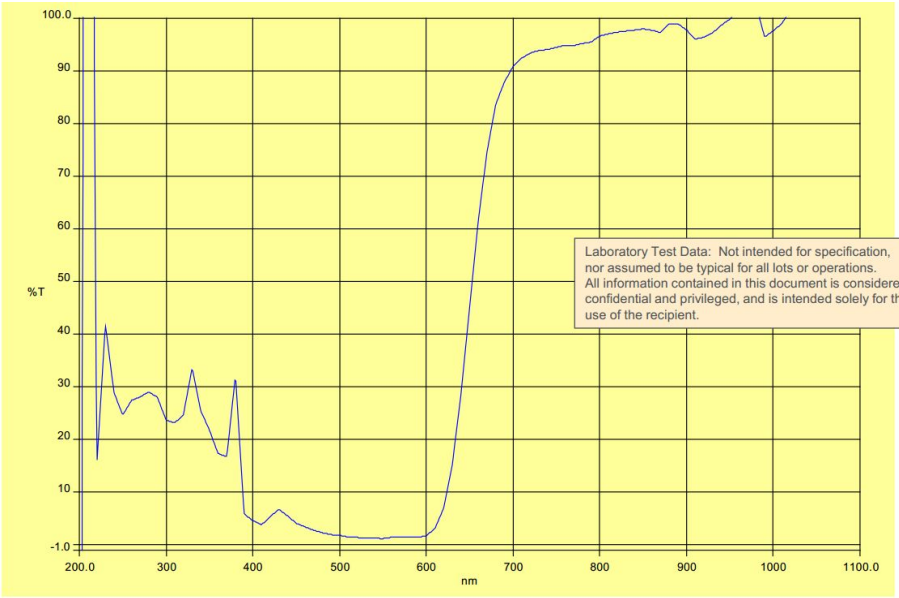

LEXAN Resin Transmission vs. Frequency
Color Code: 71509
Color Description: IR Transmitting Black

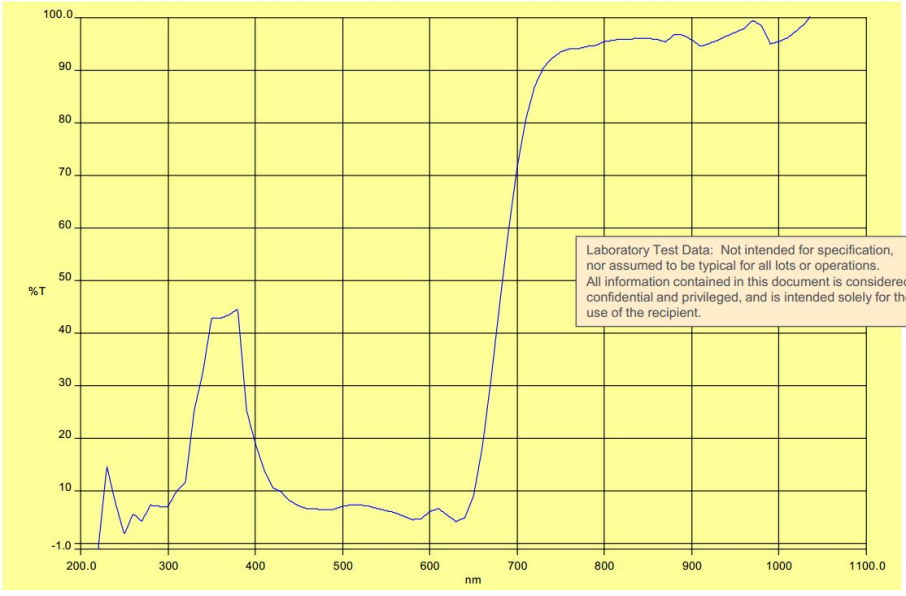

LEXAN Resin Transmission vs. Frequency
Color Code: 71563
Color Description: IR Transmitting Black

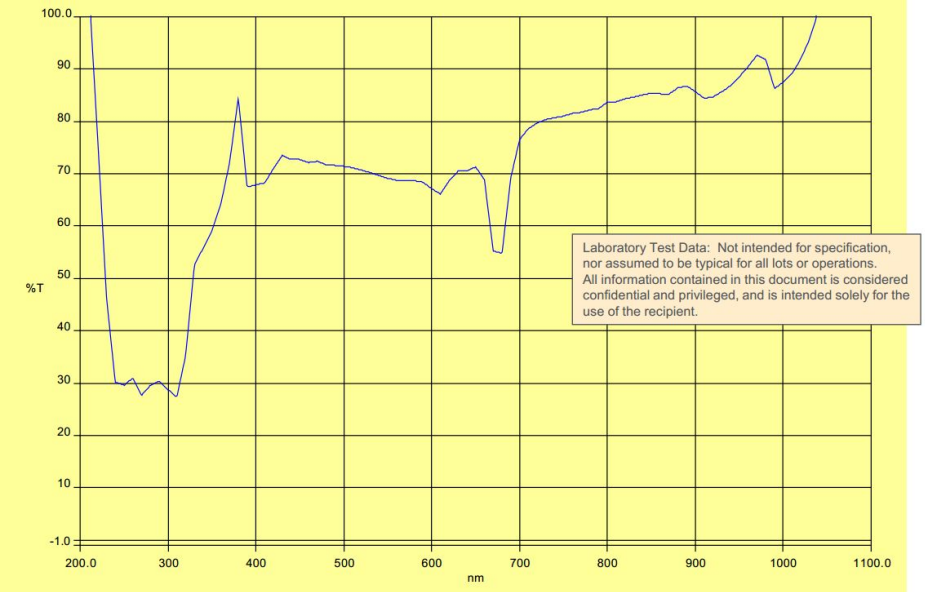

LEXAN Resin Transmission vs. Frequency
Color Code: BK1091T
Color Description: IR Transmitting Black

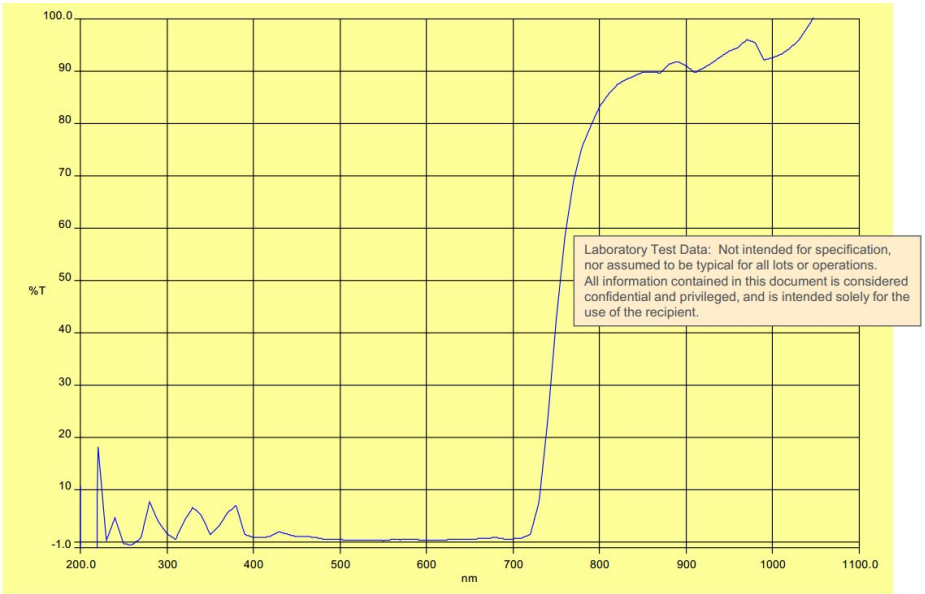

LEXAN Resin Transmission vs. Frequency
Color Code: BK1A184T
Color Description: IR Transmitting Black

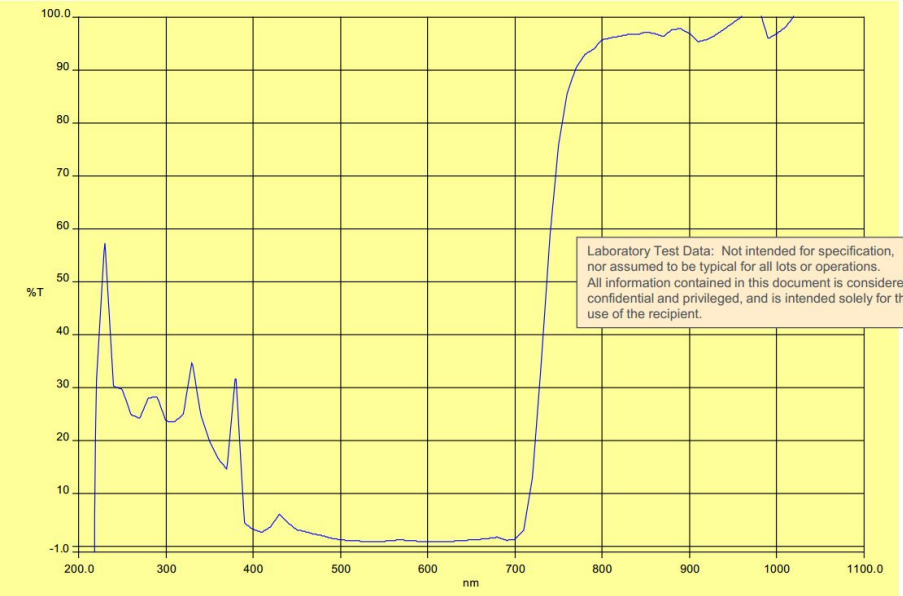

LEXAN Resin Transmission vs. Frequency
Color Code: BK1E008T
Color Description: IR Transmitting Black

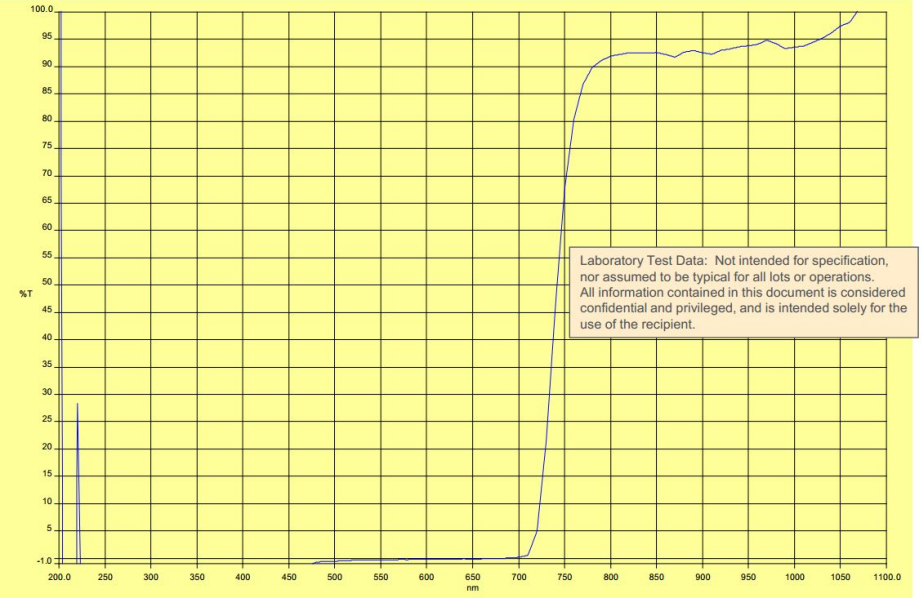

LEXAN Resin Transmission vs. Frequency
Color Code: BK1E092T
Color Description: IR Transmitting Black

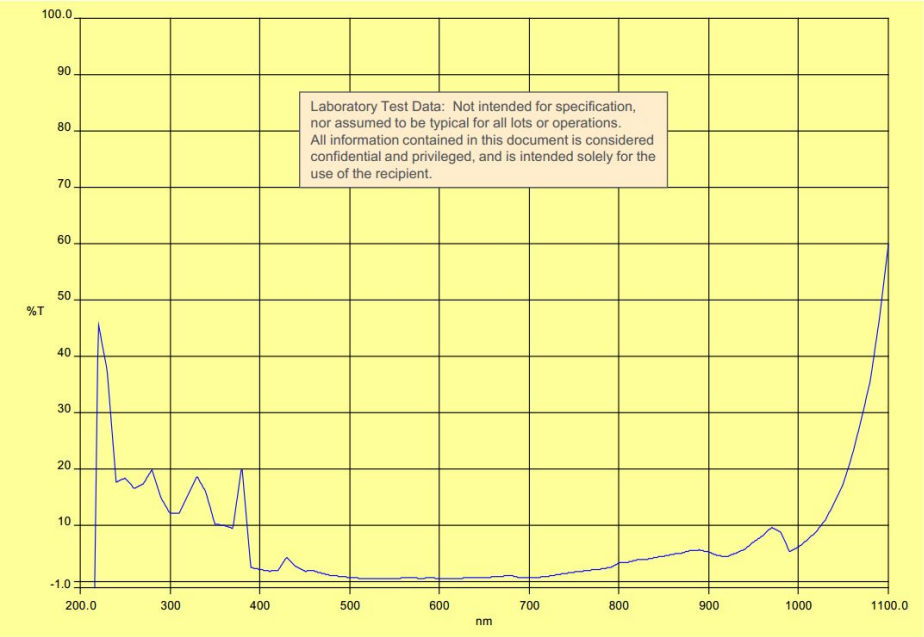

LEXAN Resin Transmission vs. Frequency
Color Code: BK1E117T
Color Description: IR Transmitting Black

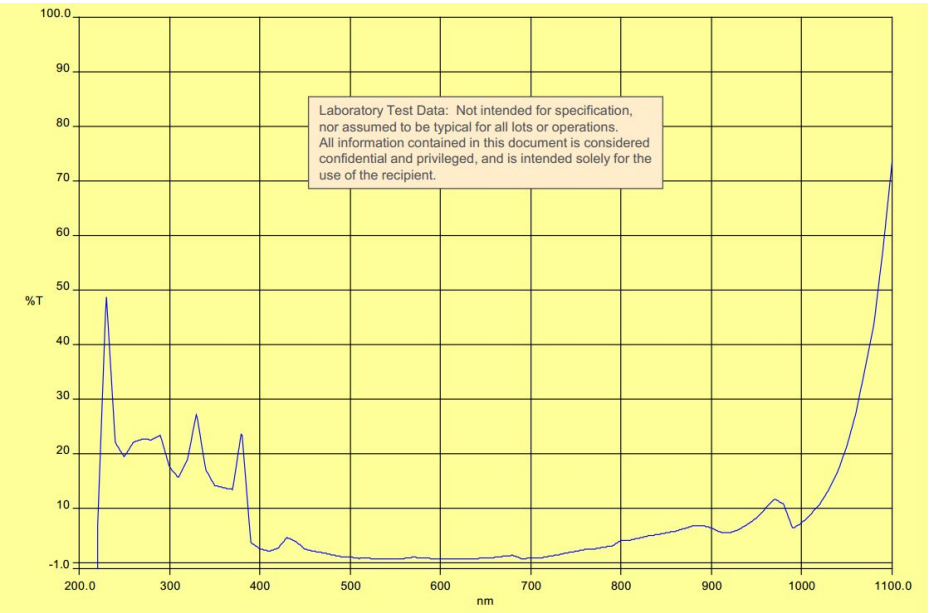

LEXAN Resin Transmission vs. Frequency
Color Code: BK1E118T
Color Description: IR Transmitting Black

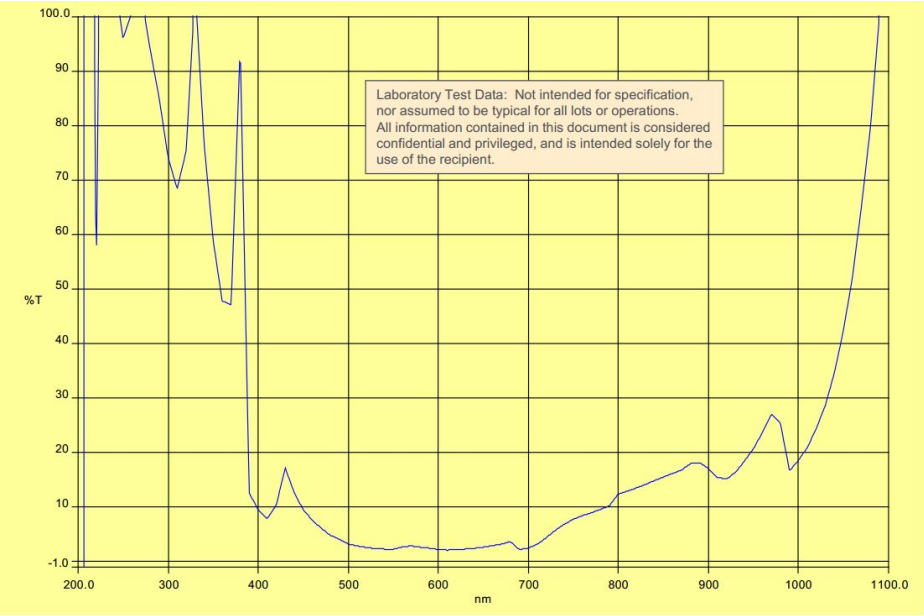

LEXAN Resin Transmission vs. Frequency
Color Code: GY1D740T
Color Description: IR Transmitting Dark Gray

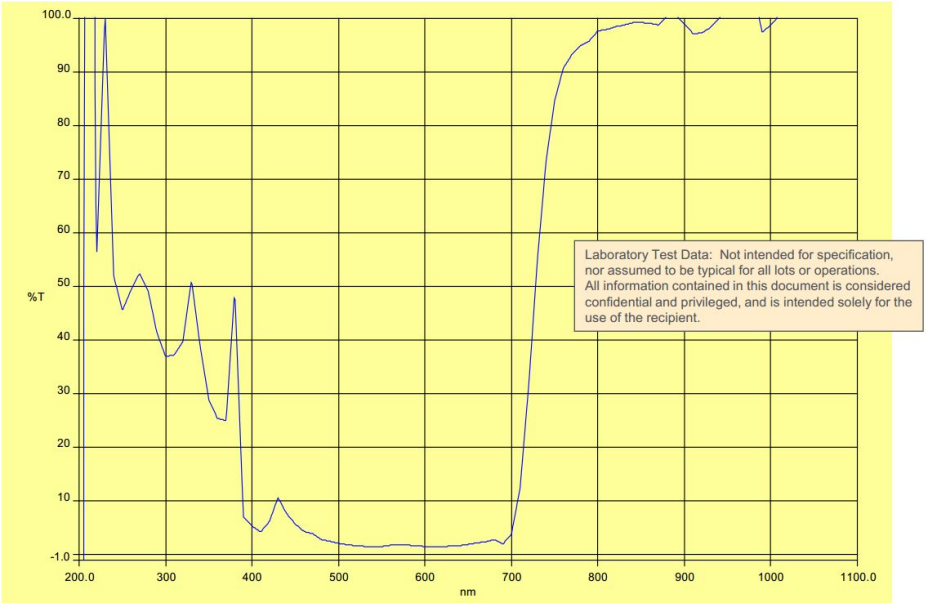

LEXAN Resin Transmission vs. Frequency
Color Code: GY4E343T
Color Description: IR Transmitting Gray